

# PCCP

Accepted Manuscript



This is an *Accepted Manuscript*, which has been through the Royal Society of Chemistry peer review process and has been accepted for publication.

*Accepted Manuscripts* are published online shortly after acceptance, before technical editing, formatting and proof reading. Using this free service, authors can make their results available to the community, in citable form, before we publish the edited article. We will replace this *Accepted Manuscript* with the edited and formatted *Advance Article* as soon as it is available.

You can find more information about *Accepted Manuscripts* in the [Information for Authors](#).

Please note that technical editing may introduce minor changes to the text and/or graphics, which may alter content. The journal's standard [Terms & Conditions](#) and the [Ethical guidelines](#) still apply. In no event shall the Royal Society of Chemistry be held responsible for any errors or omissions in this *Accepted Manuscript* or any consequences arising from the use of any information it contains.

**Adsorption according to the Langmuir-Freundlich model is the detection mechanism of the antigen p53 for early diagnosis of cancer**

Juliana Coatrini Soares<sup>1\*</sup>, Andrey Coatrini Soares<sup>1</sup>, Paulo Augusto Raymundo Pereira<sup>2</sup>,  
Valquiria da Cruz Rodrigues<sup>1</sup>, Flavio Makoto Shimizu<sup>1</sup>, Matias Eliseo Melendez<sup>3</sup>,  
Cristovam Scapulatempo Neto<sup>3,4</sup>, André Lopes Carvalho<sup>3</sup>, Fábio L. Leite<sup>5</sup>, Sergio A.S.  
Machado<sup>2</sup>, Osvaldo N. Oliveira Jr<sup>1</sup>

<sup>1</sup>*São Carlos Institute of Physics, University of São Paulo, 13560-970 São Carlos-SP, Brazil*

<sup>2</sup>*São Carlos Institute of Chemistry, University of São Paulo, 13560-970 São Carlos-SP, Brazil*

<sup>3</sup>*Molecular Oncology Research Center, Barretos Cancer Hospital, Barretos-SP, Brazil*

<sup>4</sup>*Department of Pathology, Barretos Cancer Hospital, Barretos-SP, Brazil*

<sup>5</sup>*Federal University of São Carlos, Sorocaba- SP, Brazil*

\*corresponding author: jucoatrini@yahoo.com.br

**Abstract**

Biosensors for early detection of cancer biomarkers normally depend on specific interactions between such biomarkers and immobilized biomolecules in the sensing units. Though these interactions are expected to yield specific, irreversible adsorption, the underlying mechanism appears not to have been studied in detail. In this paper, we show that adsorption explained with the Langmuir-Freundlich model is responsible for detection of the antigen p53 associated with various types of cancer. Irreversible adsorption was proven between anti-p53 antibodies immobilized in the biosensors and

the antigen p53, with the adequacy of the Langmuir-Freundlich model being confirmed with three independent experimental methods, *viz.* polarization-modulated infrared reflection absorption spectroscopy (PM-IRRAS), nanogravimetry with a quartz crystal microbalance and electrochemical impedance spectroscopy. The method based on this irreversible adsorption was sufficiently sensitive (limit of detection of 1.4 pg/mL) for early diagnosis of Hodgkin lymphoma, pancreatic and colon carcinomas, bladder, ovarian and lung cancers, and could distinguish between MCF7 cells containing the antigen p53 from Saos-2 cells that do not contain it.

Keywords: models for adsorption, Langmuir-Freundlich, biosensors, detection of cancer biomarkers, electrochemical impedance spectroscopy

## 1 Introduction

The detection of biomarkers has been consolidated as suitable for early diagnosis of various types of cancer, since cancer cells secrete specific biomolecules that may be identified long before the symptoms of the disease are manifested<sup>1</sup>. This has prompted a worldwide search for appropriate biomarkers, as is the case of the gene p53, which is a tumor suppressor gene located on the short arm of chromosome 17<sup>2</sup>. Inactivation of p53 is found in many types of tumors, including those related to adrenocortical, breast, leukemia, lymphomas, lung, gastrointestinal and skin cancers, resulting from mutations that cause loss of wild-type p53 activity<sup>3</sup>. Various are the methods to detect biomarkers, most of which rely on the specific interaction between a biomolecule immobilized in the biosensor and the biomarker in the sample under analysis<sup>4</sup>. Because in many cases the biomolecule-analyte pair consists of antibodies and antigens, these biosensors are referred to as immunosensors<sup>4</sup>.

The Enzyme Linked Immuno Sorbent Assay (ELISA) test<sup>5</sup> is perhaps the most widely used assay for antigen detection, in spite of its high cost and limited sensitivity that may hamper its use for detecting cancer at early stages<sup>6</sup>. Immunosensors have also been produced whose principle of detection may involve electrochemistry<sup>7,8,9</sup>, chemiluminescence<sup>10,11</sup>, piezoelectricity<sup>12,13</sup>, surface plasmon resonance,<sup>14,15,16</sup> and impedance spectroscopy<sup>17,18,19</sup> including its electrochemical version<sup>20</sup>. The sensing units for these immunosensors are normally made with nanostructured films, such as self-assembled monolayers (SAMs)<sup>21,22</sup>, and layer-by-layer (LbL) films<sup>23,24,25</sup>, which are suitable for preserving the activity of the biomolecules immobilized. For the antigen p53, in particular, biosensors have been made mostly with DNA modified electrodes, as

with films containing composite nanofibers with polymers and carbon nanotubes<sup>26</sup>, silver nanoparticles<sup>27</sup> and a DNA-binder in a MOSFET (metal oxide semiconductor field-effect transistor) device<sup>28</sup>. Other immunosensors for detecting the p53 biomarker include the combination of immunomagnetic separation and electrochemiluminescence<sup>29</sup> and deflection of microcantilevers with piezoresistors<sup>30,31,32</sup>.

The strong, specific interaction between antigens and antibodies is an indication that the mechanism behind biosensing in an immunosensor is irreversible adsorption. Indeed, there is ample experimental evidence from earlier work<sup>17,19,33</sup> for such an adsorption, obtained with distinct methods, including with atomic force microscopy<sup>34</sup> and polarization-modulated infrared reflection absorption spectroscopy (PM-IRRAS). However, a systematic study about adsorption processes appears to be lacking, which is the main purpose of the present paper.

Models for adsorption have been proposed for almost a century since the pioneering contribution from Langmuir<sup>35</sup>. They were developed primarily for adsorption of atoms or small molecules, depending essentially on whether the adsorbing species interact among themselves and whether monolayers or multilayers are formed on the surface. The simplest Langmuir model quantifies how a monolayer of an adsorbate is formed on a given surface based on an equilibrium of ions between the solid and liquid phases<sup>35,36,37</sup>. Langmuir adsorption isotherms are then obtained from plots of the amount of material adsorbed versus its concentration in solution. Since the simplifications in the Langmuir model are severe, modifications have been introduced to generate more realistic models. The Langmuir-Freundlich model<sup>36,38,39</sup>, for instance,

considers adsorption to occur in multiple layers, being useful to describe adsorption on heterogeneous surfaces.

In spite of the over simplifications in these models, they have been shown applicable to adsorption of macromolecules, such as semiconducting polymers in layer-by-layer (LbL) films<sup>40</sup>. In this paper, we apply the most simple models of adsorption to show that the detection mechanism for the antigen p53 can be explained with the Langmuir-Freundlich model. This hypothesis was proven through three techniques, namely PM-IRRAS, nanogravimetry using a quartz crystal microbalance (QCM), and electrochemical impedance spectroscopy, using biosensors with an architecture containing immobilized anti-p53 antibodies in a self-assembled monolayer (SAM). We also demonstrate that the irreversible adsorption between anti-p53 antibodies and p53 antigens is sufficiently specific to yield highly sensitive and selective biosensors, capable of detecting the biomarker at early stages of various types of cancer.

## 2 Experimental

The sensing units were fabricated using 11-mercaptoundecanoic acid (Sigma Aldrich, USA), N-Hydroxysuccinimide (Sigma Aldrich, USA), 1-Ethyl-3-(3-dimethylaminopropyl)carbodiimide (Sigma Aldrich, USA), p53 antibody (Dako), bovine serum albumin (BSA) (Sigma Aldrich, USA), while the samples to be detected consisted of antigen p53 (ABCAM, UK) in a phosphate buffered saline (PBS) solution, pH 7.4. In addition, whole cell lysates from MCF7 (p53-expressing) and Saos-2 (p53-null) cell lines were also used as p53 antigen sources. Whole cell lysates were obtained by three cycles of freeze-thaw and stored at -80°C.

The nanostructured films were deposited on gold, in the following sequence:

1) a thiol self-assembled monolayer (SAM) of *11mercaptoundecanoic acid* (MUA) was adsorbed on gold by immersing the solid support into a .5.0 mmol/L solution for 24 h. It was then activated for an effective adsorption of p53 antibodies by incubation into 0.1 mol/L N-Hydroxysuccinimide (NHS) and 0.1 mol/L 1-Ethyl-3-(3-dimethylaminopropyl)carbodiimide (EDC) for 24 h.

2) The MUA-NHS-EDC film was coated with a layer of p53 antibodies by immersion into 25  $\mu$ L of antibody (AB) solution AB:PBS (1:1000) at 37°C for 10 min under controlled humidity.

3) In order to avoid non-specific adsorption of the antigens in the detection measurements, the film containing anti-p53 antibodies was immersed into a BSA 1% solution.

Detection was carried out with three different techniques, namely PM-IRRAS, QCM and electrochemical impedance spectroscopy. In all cases, the sensing unit (MUA-NHS-EDC/anti p53-BSA) was exposed to the sample in PBS (either antigen p53 in PBS or whole cell lysates), and left for 10 min for adsorption of the analyte at 25°C after which it was washed with PBS solution and dried. For PM-IRRAS and QCM, therefore, the measurements were performed with solid films. PM-IRRAS measurements were performed using a KSV PMI 550 Instrument, Helsinki, Finland, with spectral resolution of 8  $\text{cm}^{-1}$  and an incidence angle of 80°. QCM measurements were carried out with a QCM 200, Stanford Research Systems Inc, with the nanostructured film (MUA-NHS-EDC/anti p53-BSA) adsorbed on a quartz crystal coated with gold.

The electrochemical impedance measurements were performed with a PGSTAT 204, Autolab electrochemical system (Eco Chimie, Netherland) and controlled by NOVA software. All measurements were carried out in a 25 mL thermostated glass cell

at 25°C, with a three-electrode configuration: the nanostructured film deposited onto a gold interdigitated electrode as the working electrode (geometric area 9.5 mm<sup>2</sup>), a Ag/AgCl (3 mol/L KCl) as a reference and a platinum foil (1.0 cm<sup>2</sup>) as an auxiliary electrode. The solution within the cell was neither stirred nor aerated during the measurements. Electrochemical impedance spectroscopy (EIS) data were acquired in the frequency range between 0.1 Hz and 100 kHz with amplitude of 10 mV and under open circuit potential (OCP) conditions in solution containing 5.0 mmol/L of K<sub>3</sub>[Fe(CN)<sub>6</sub>]/K<sub>4</sub>[Fe(CN)<sub>6</sub>] (Sigma Aldrich, USA).

It is worth emphasizing that in all detection measurements, with the three techniques, the MUA-NHS-EDC/anti p53-BSA film was washed after being exposed to the samples under analysis, in order to remove non-adsorbed molecules. Therefore, because the MUA-NHS-EDC/anti p53-BSA film is highly stable, its properties should only be affected if irreversible adsorption of molecules from the sample occurred.

The impedance data were treated with information visualization<sup>41,42</sup> methods implemented in a free software suite referred to as Projection Explorer for Sensors (*PEx-Sensors*)<sup>41,42</sup>. Specifically, the spectra for the imaginary component of the impedance obtained from EIS measurements were analyzed using the projection technique *Interactive Document Mapping* (IDMAP)<sup>43</sup>, which uses Euclidean distances for the mapping of the data points. With a projection technique, we assume that the original data ( $Z''$  vs frequency curves in our case) are represented by  $X=\{x_1, x_2, \dots, x_n\}$ , where the dissimilarity between two samples (i and j) is given by  $\delta(x_i, x_j)$ , and plotted on a 2D space where the distance between two projected data points ( $y_i$  and  $y_j$ ) is

$d(y_i - y_j)$ . With IDMAP, in particular, the projection is made using an injective function  $f: X \rightarrow Y$ , which minimizes  $|\delta(x_i, x_j) - d(y_i - y_j)| \forall x_i, x_j \in X$ , defined in Eq. (7)<sup>43</sup>

$$S_{IDMAP} = \frac{\delta(x_i, x_j) - \delta_{\min}}{\delta_{\max} - \delta_{\min}} - d(y_i, y_j) \quad (1)$$

where  $\delta_{\max}$  and  $\delta_{\min}$  are the maximum and minimum distances between data instances.

The PM-IRRAS, QCM and EIS signals were analyzed with regard to adsorption of the analyte on the immunosensor. The relationship observed between signals and adsorption of the analyte could be explained with a Langmuir-Freundlich model<sup>36,38,39</sup> according to which the amount of material adsorbed is given by equation 2

$$q = \frac{Q_m (K_a C_{eq})^n}{(K_a C_{eq})^n + 1} \quad (2)$$

where  $q$  is the amount of adsorbed material on the substrate at equilibrium,  $Q_m$  is the adsorption capacity, which is related to the number of available binding sites,  $C_{eq}$  is the aqueous phase concentration at equilibrium,  $K_a$  is the affinity constant for adsorption and  $n$  is the index of heterogeneity.

### 3 Results and Discussion

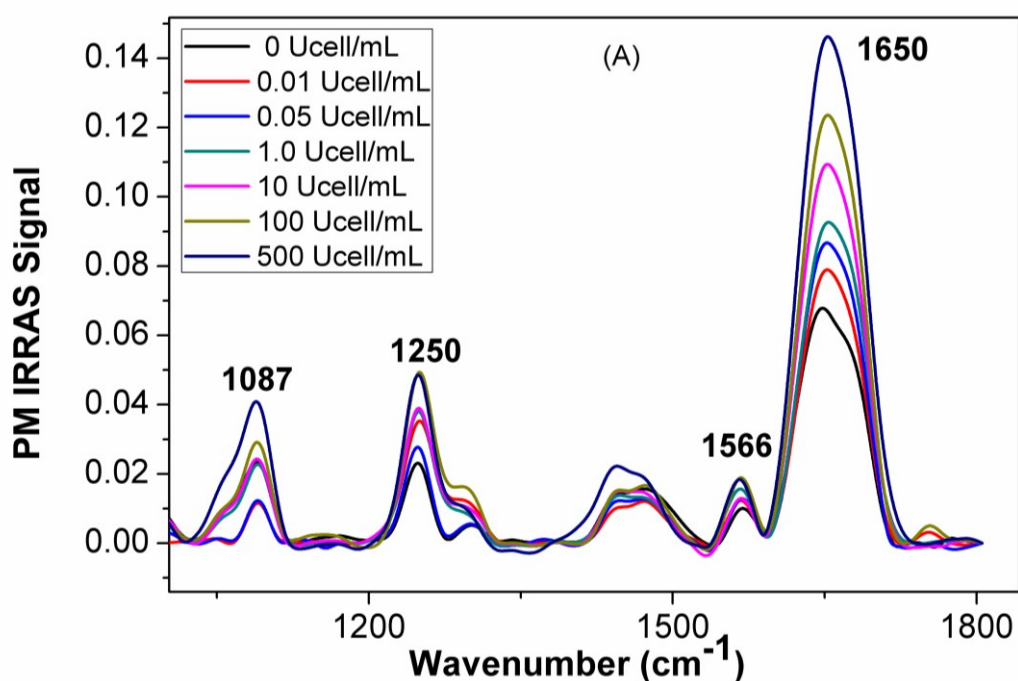
The purpose of this study was twofold. First, we wished to verify the adsorption mechanisms responsible for the specific interaction between antibodies and antigens,

which allows for the fabrication of efficient immunosensors. Second, we demonstrate that the robust immunosensors can be produced for the antigen p53 detection.

### **Specific antigen-antibody adsorption as the detection mechanism**

The PM-IRRAS spectra for the MUA-NHS-EDC/anti p53-BSA film adsorbed on gold, displayed in Figure 1A with base line correction, exhibits the following bands: i) amide I between 1600-1700  $\text{cm}^{-1}$  assigned to vibrational modes of carbonyl (C=O) from the carboxylic acid groups in the amino acids; amide II between 1500-1600  $\text{cm}^{-1}$ , where 60% of the potential energy in the vibration are associated with the N-H bond while the remaining 40% are related to the C-N bond stretch of amide groups; iii) at 1440, 1260 and 1087  $\text{cm}^{-1}$  assigned to aliphatic amines, C-O-H groups and the angular deformation of  $-\text{CH}_2-$  groups, respectively, all from proteins<sup>17,44,45</sup>. Note that no bands are assigned to MUA and NHS-EDC since the baseline correction was made taking the spectrum of a MUA-NHS-EDC film as the reference. The bands are all directed upward, which means that the dipole moments of the groups involved are preferably oriented on the film plane. Since the bands in this region of the spectrum originate from proteins, all of them were affected by exposing the MUA-NHS-EDC/anti p53-BSA film to the antigen p53. We took the amide band centered at 1650  $\text{cm}^{-1}$  for a quantitative analysis, and as expected the area under the band increased with the concentration of p53, thus reflecting stronger adsorption. This is best illustrated in the plot of Figure 1B where the area is seen to increase with concentration as in other biosensors based on adsorption of the analyte<sup>33</sup>. It results from saturation of available antibody molecules to which the antigen molecules could bind. The concentration dependence in Figure 1B may be explained with the Langmuir-Freundlich model, as shown by the adequate fitting of the data. The detection limit (LOD) calculated from the linear part in the beginning of the curve in

Figure 1B for the area below the band of  $1650\text{ cm}^{-1}$  is  $0.136\text{ Ucell/mL}$ . In subsidiary analysis, we tried to fit the data with the Langmuir model, but the quality of the fitting was inferior to that with the Langmuir-Freundlich model. It should be stressed that in this analysis we assumed that the intensity of specific PM-IRRAS bands was proportional to the quantity of p53 adsorbed. This is only the case if there are no changes in molecular orientation of the groups leading to the bands, since the band intensity does depend on such orientation.



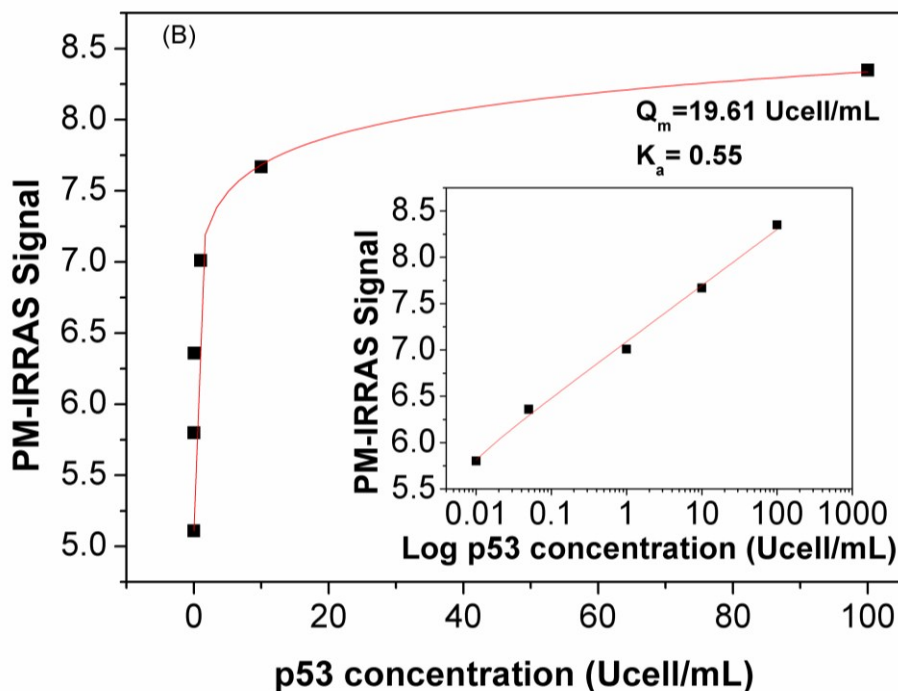


**Figure 1.** (A) PM-IRRAS spectra for the MUA-NHS-EDC/anti p53-BSA film adsorbed on gold, before (black line) and after exposure to the antigen p53 sample at various concentrations (colored lines). (B) Area under the  $1653\text{ cm}^{-1}$  band versus concentration of antigen p53 in the cell lines, with a dependence fitted with the Langmuir-Freundlich model.

A detection mechanism based on adsorption of the analyte, as shown to be the case in the PM-IRRAS spectra, can also be investigated with a QCM. Indeed, Figure 2a shows the frequency shift in the resonance of the crystal quartz coated with the MUA-NHS-EDC/anti p53-BSA film when the concentration of antigen p53 in the cell lines was varied. Using the Sauerbrey equation<sup>46</sup>, we calculated the mass of p53 antigen adsorbed in each step (Figure 2a) for adsorption during 130 s. Moreover, a sharp increase in adsorbed mass followed by a saturation was observed (Figure 2b), fitted

with a Langmuir-Freundlich isotherm<sup>36,38,39,47</sup>, again consistent with saturation of available sites as shown for the PM-IRRAS data in Figure 1B.

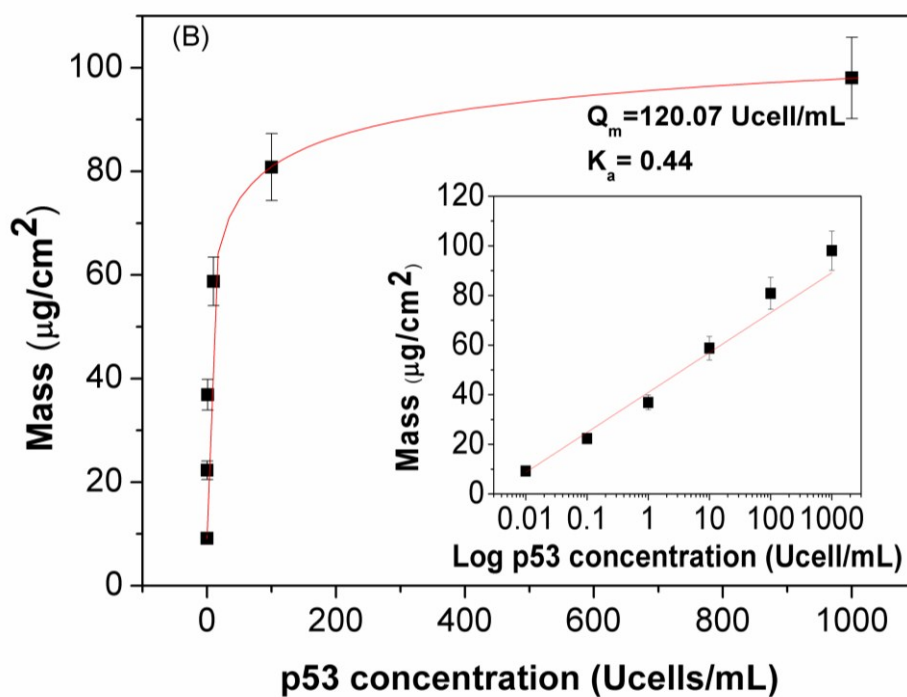
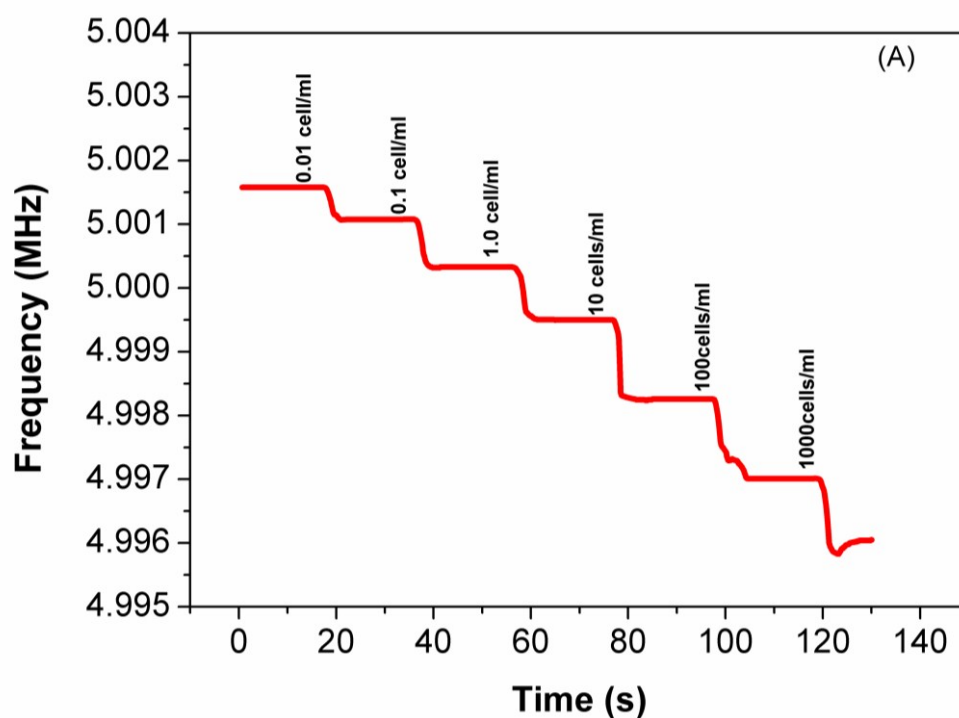


**Figure 2.** (A) Kinetics of adsorption of cell lines containing antigen p53 with adsorption steps of 130 s, shown as a decrease in the resonance frequency of the quartz crystal. (B) Plot of the adsorbed mass versus concentration of antigen p53 in the cell lines, with fitting using the Langmuir-Freundlich model.

The suitability of the adsorption mechanism for detecting antigen p53 allows one to produce less sophisticated immunosensors, with cheaper techniques than those discussed above. Here we use electrochemical impedance spectroscopy (EIS), which is useful to investigate molecular interactions at interfaces<sup>48</sup>. We should keep in mind, nevertheless, that electrical properties leading to the impedance of a given system may be affected by any change in the analyte as well as in the film. It is therefore a non-specific method, but there is expectation that it will be suitable to distinguish between samples containing the antigen p53 from others that do not, owing to the experimental procedure adopted to wash the MUA-NHS-EDC/anti p53-BSA film after each exposure to a sample under analysis. Indeed, the Nyquist plots for the impedance data with the MUA-NHS-EDC/anti p53-BSA film (Figure 3A) indicate considerable changes when the concentration of antigen p53 varies for both cell line lysates.

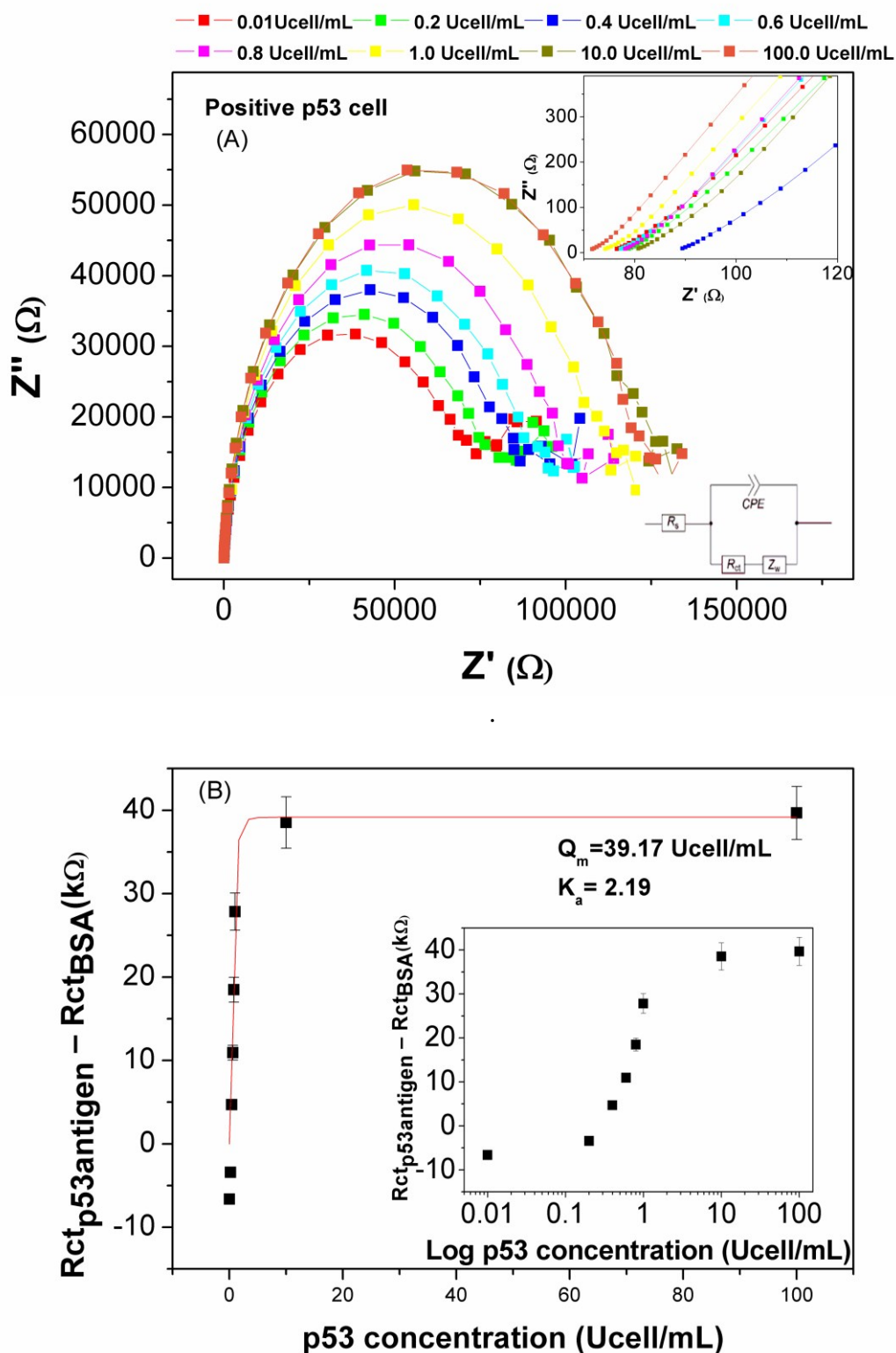


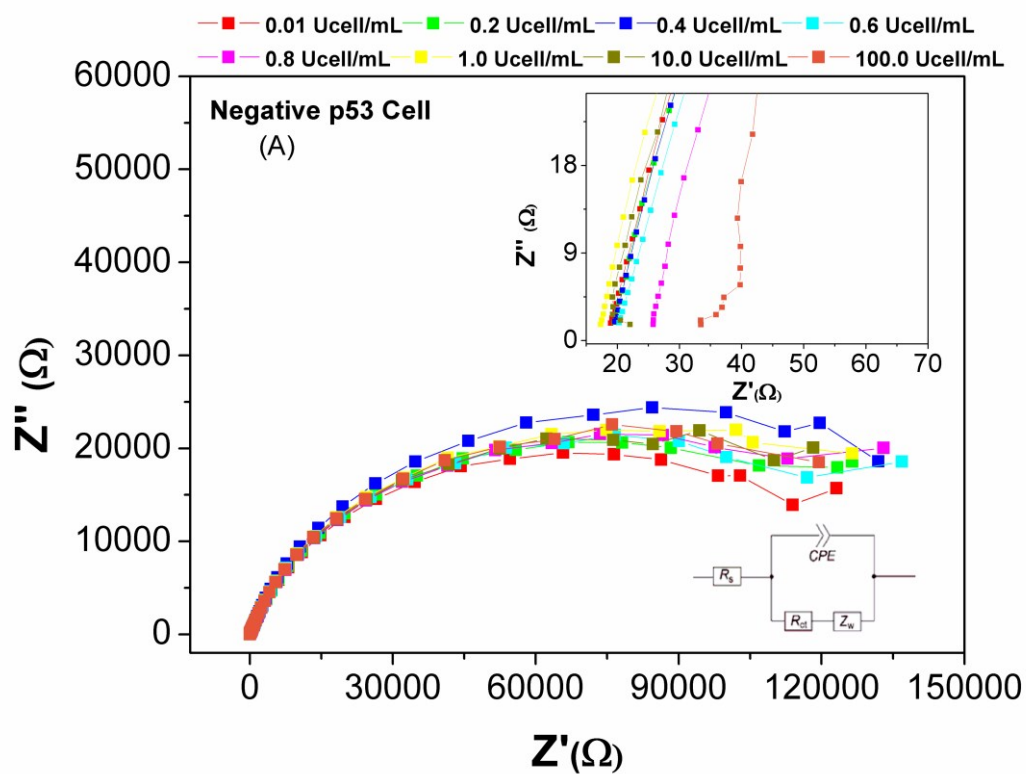
**Figure 3.** (A) Nyquist plots of the impedance spectra from 100 kHz to 1 Hz for a gold electrode modified with a MUA-NHS-EDC/anti p53-BSA film in  $K_3Fe(CN)_6$  and  $K_4Fe(CN)_6$  following exposure to different concentrations of cells containing the antigen p53

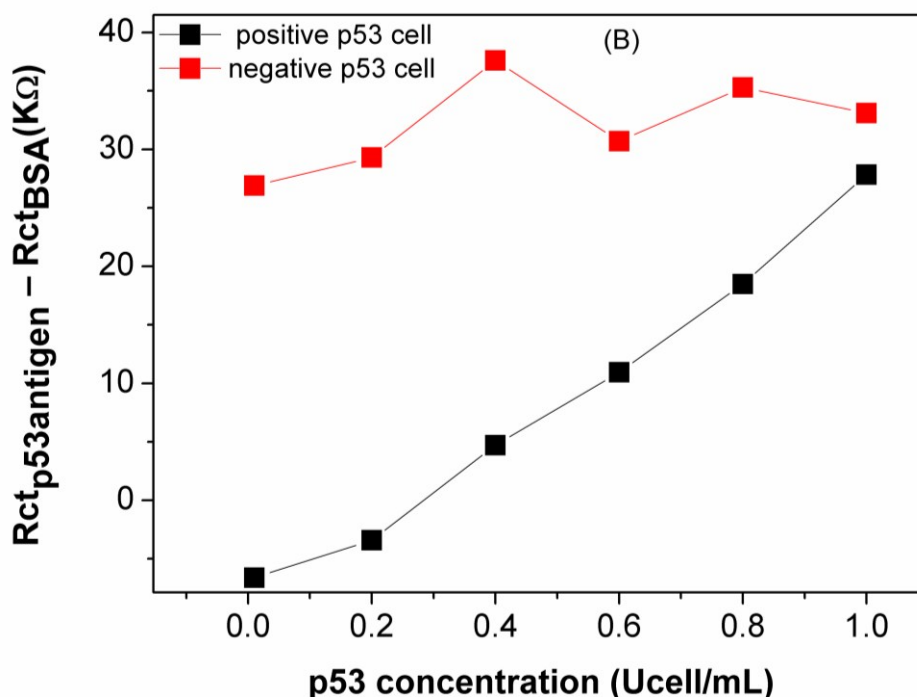
(positive cells). (B) Plot of the relative change in  $R_{ct}$  against the concentration of the positive cells, which is fitted with the Langmuir-Freundlich model.

A more straightforward manner to probe the concentration dependence is to analyze the Nyquist plots using a Randles equivalent circuit from which several parameters may be inferred. The use of such a circuit, as the one shown in the inset of Figure 3A, is justified in cases where the total impedance depends on several parameters and may not be easily related to molecular mechanisms. The Nyquist plots were fitted with the Electrochemistry-ZView 2 software-free and applying a Randles circuit  $RS(CPE[R_{ct}ZW])$  to determine the parameter  $R_{ct}$ . The components of the Randles circuit are: electrolyte resistance ( $R_s$ ), charge transfer resistance ( $R_{ct}$ ), and a constant phase element (CPE), to account for capacitance dispersion.  $R_s$  and  $Z_w$  represent the bulk properties of the electrolyte solution and diffusion of the analyte toward the film surface, respectively. From the plots in Figure 3A it is clear that  $R_{ct}$  varies with the concentration, whose increase is shown in Figure 3B. Consistent with the PM-IRRAS and QCM data, saturation of the change in  $R_{ct}$  is observed at very high concentrations, and the curve can be fitted with the Langmuir-Freundlich model. Taking the part of the curve at low concentrations, which is practically linear, one may obtain the limit of detection of 0.151 Ucell/mL, using the IUPAC method ( $LOD = 3S_B/S$ ) where  $S_B$  is the standard deviation of 10 measurements taken from the signal obtained from the blank (a solution identical to that analysed but without the analyte) and  $S$  the slope of the calibration curve (sensitivity of the analytical method)<sup>49,50</sup>.

In contrast, for the p53-null Saos-2 cell lysate used at several dilutions, the Nyquist plots in Figure 4A practically coincide with each other. Figure 4B indeed

shows almost no change in  $R_{ct}$  with the varying concentration for this p53-null cell lysate, where the behavior for the p53-expressing MCF7 cells from Figure 3B is reproduced for comparison.

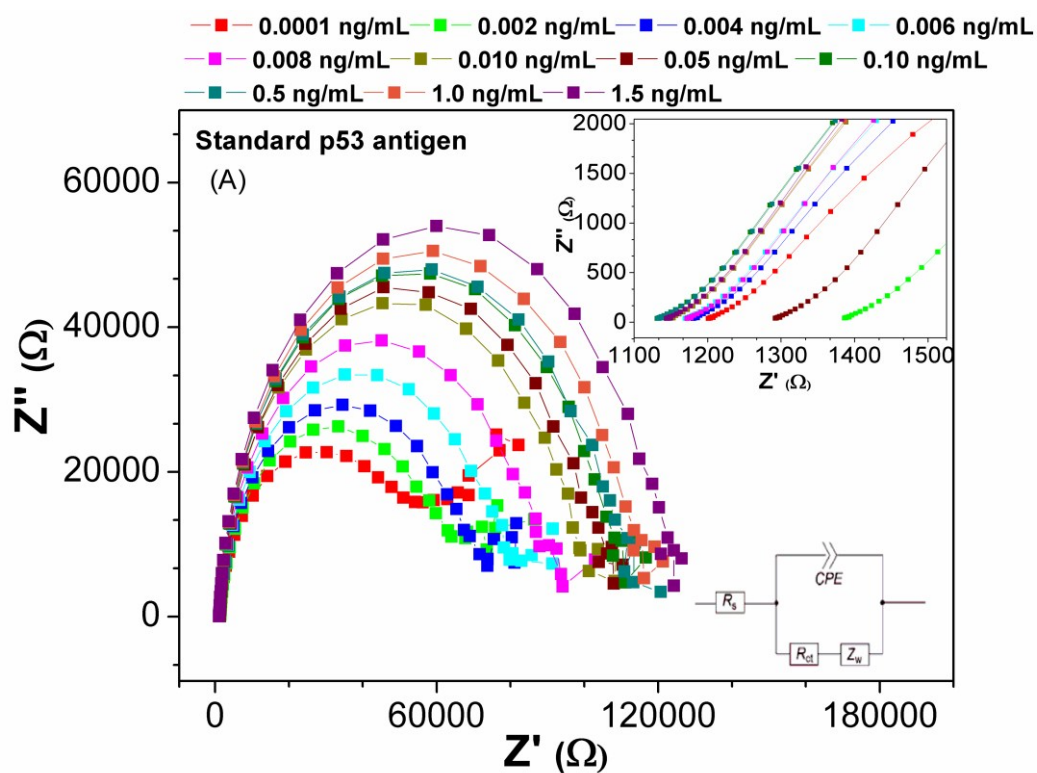




**Figure 4.** (A) Nyquist plots of the impedance spectra from 100 kHz to 1 Hz for a gold electrode modified with a MUA-NHS-EDC/anti p53-BSA film in  $K_3Fe(CN)_6$  and  $K_4Fe(CN)_6$  following exposure to different concentrations of cells that did not contain the antigen p53 (negative cells). (B) Plot of the relative change in  $R_{ct}$  against the concentration of negative cells. The plot for positive cells from Figure 3 is shown for comparison.

In order to verify if the sensitivity of the immunosensor made with the MUA-NHS-EDC/anti p53-BSA film should be sufficient for detecting the antigen p53 as it occurs in different types of cancer, we performed a series of subsidiary experiments with synthetic samples. That is to say, rather than using cell line lysates containing the antigen p53 biomarker, we deliberately added this biomarker commercially acquired to a PBS buffer. The Nyquist plots obtained with the MUA-NHS-EDC/anti p53-BSA film exposed to these samples with different p53 concentrations are shown in Figure 5A. The charge transfer resistance  $R_{ct}$  varies with the antigen p53 concentration in Figure 5B much in the same way as for the positive cells in Figure 3B. From the linear part of this

concentration dependence curve, we obtained a limit of detection of 0.0014 ng/mL (1.4 pg/mL). This sensitivity is actually sufficient to detect the antigen p53 in real cases, as the threshold for detection is considerably higher. Indeed, this threshold is 30 pg/mL for Malignant lymphoma, 50 pg/mL in Hodgkin lymphoma; 50 pg/mL in Pancreatic carcinoma; 50 pg/mL in Bladder cancer; 200 pg/mL in Ovarian cancer; 50 pg/mL in Colon carcinoma; 50 pg/mL in Lung cancer and 10 pg/mL in Small-cell lung cancer<sup>49</sup>.



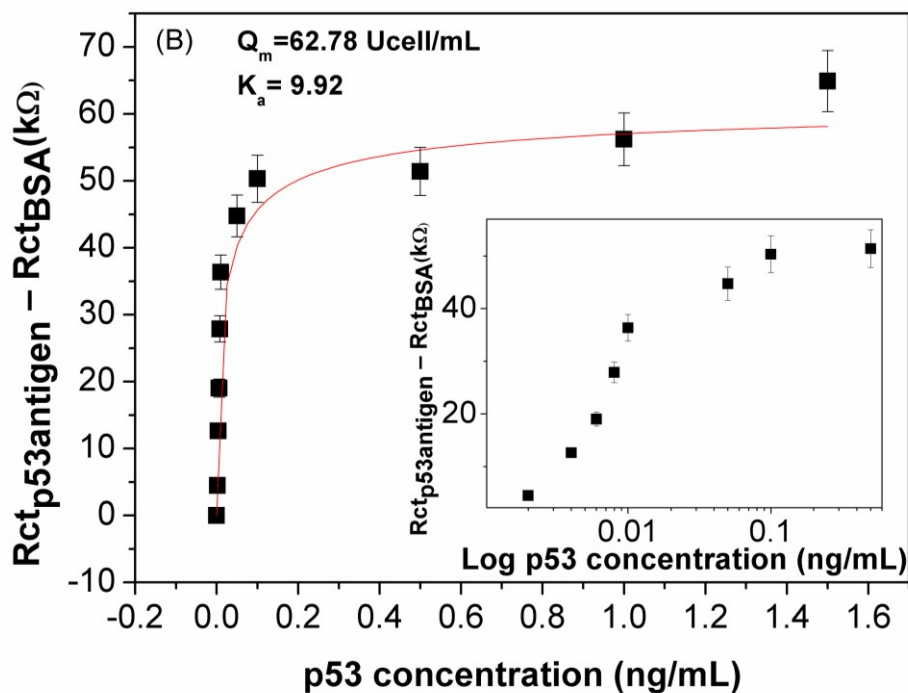


**Figure 5.** (A) Nyquist plots of the impedance spectra from 100 kHz to 1 Hz for a gold electrode modified with a MUA-NHS-EDC/anti p53-BSA film in  $K_3Fe(CN)_6$  and  $K_4Fe(CN)_6$  following exposure to standard solutions of PBS containing different concentrations of the antigen p53. (B) Plot of the relative change in  $R_{ct}$  against the concentration of the antigen p53, which was fitted with the Langmuir-Freundlich model.

### Robustness of the detection based on the Langmuir-Freundlich adsorption mechanism

One major challenge for obtaining efficient, highly selective immunosensors is to avoid non-specific adsorption. In this study, we adopted experimental procedures to guarantee that the measurements with distinct types of principles of detection were only affected by the specific antigen-antibody interaction. Specifically, the selectivity of the immunosensor made with the MUA-NHS-EDC/anti p53-BSA film was verified by exposing it to other antigens and non-specific analytes which may be contained in

patient blood samples. We used as non-specific analytes samples of p24 antigen for HIV, HCV antigen for Hepatitis C, glucose, ascorbic acid and uric acid. Figure 6 shows the charge transfer resistance calculated from the impedance data for the film exposed to each of these analytes, where one may see that only the antigen p53 gave a considerably different value from the PBS buffer. All the others had  $R_{ct}$  very close to PBS, perhaps with the exception of ascorbic acid which had some effect, though easily distinguishable from the large change for the antigen p53.

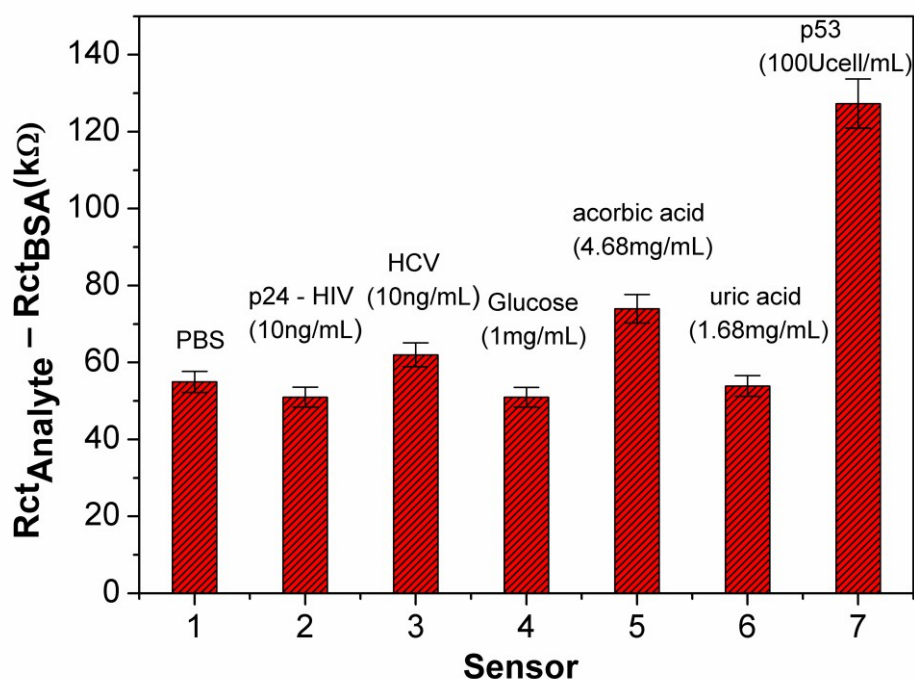


**Figure 6.** Charge transfer resistance ( $R_{ct}$ ) for an immunosensor made with a MUA-NHS-EDC/anti p53-BSA film exposed to PBS and various analytes introduced in PBS, as follows: PBS (1), antigen p24 for HIV (2), antigen for HCV (3), glucose (4), ascorbic acid (5), uric acid (6) and antigen p53 (7).

The impedance data (considering the whole spectrum for each sample) for all the samples can be visualized using multidimensional projection techniques, which have

been useful to analyze biosensing data. With this type of method, one hopes to plot similar instances from a large set of samples very close to each other, while dissimilar samples should be placed far from each other on the plot. Figure 7 shows an IDMAP plot for the imaginary component of the impedance, from which it is clear that the real samples obtained with various dilutions of cell line lysates containing the antigen p53 (referred to as positive samples and represented by the whole cell lysate of MCF7 cells) can be easily distinguished from the negative samples, made with cell line lysates (obtained from Saos-2 cells) that did not contain antigen p53. The samples with p53 antigen added to PBS (referred to as standard samples) are placed close to the positive ones, as one should expect, far from the negative samples. Furthermore, within each cluster of points (samples), distinction can be made of samples with different concentrations of p53 antigen or of the cells containing it. Note, for instance, the trends for increasing concentrations within each cluster. For the so-called negative samples, in contrast, there is no such trend since the changes observed in the electrical properties are much smaller, originating from mere fluctuations owing to the dispersion in the samples.

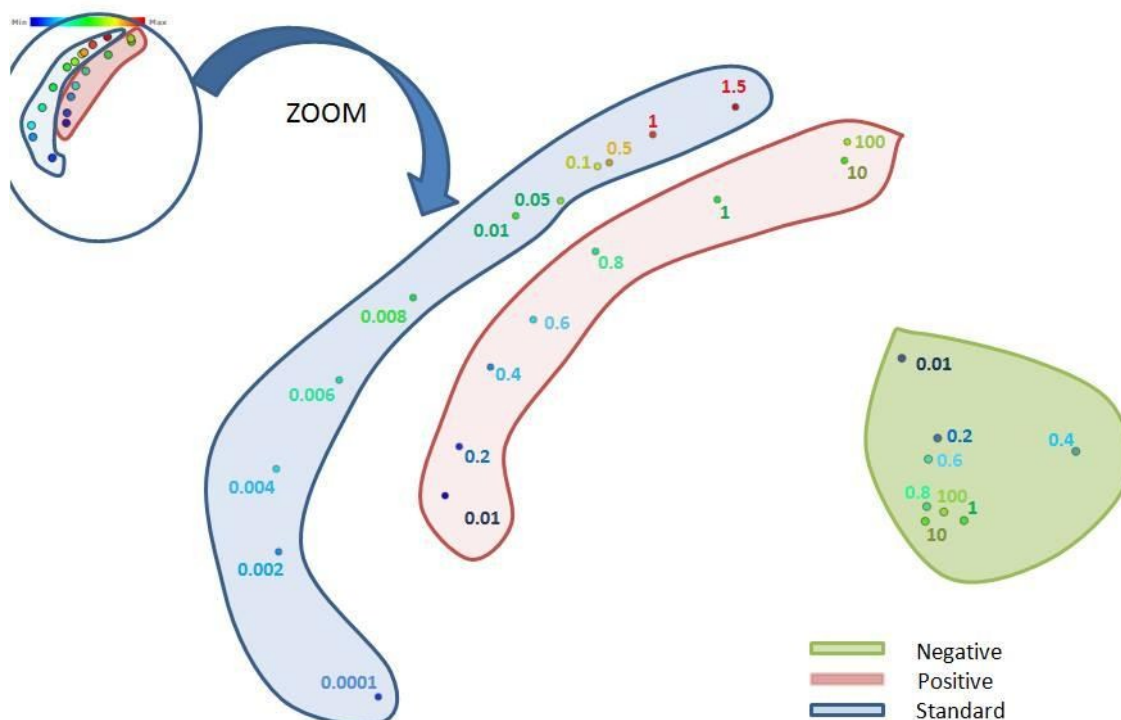


**Figure 7.** IDMAP plot for the  $Z''$  vs. frequency curves for different concentrations of cell lines containing the antigen p53 (referred to as positive) and of cell lines that did not contain p53 (negative). Also shown are standard samples made with PBS buffer to which distinct concentrations of antigen p53 were added.

#### 4 Conclusion

We have confirmed that adsorption of the antigen biomarker p53 onto immobilized antibodies is the main mechanism responsible for the high sensitivity of an immunosensor made with nanostructured films. To the best of our knowledge, ours was the first attempt to model the adsorption mechanism, which can be explained with the simple Langmuir-Freundlich model. The latter result was confirmed with three different techniques, namely PM-IRRAS, nanogravimetry and electrochemical impedance spectroscopy. In addition to obtaining essentially the same adsorption behavior in these three techniques, the sensitivity in all cases was sufficiently high for allowing to

distinguish between cell lines containing the p53 antigen or not. Moreover, experiments with electrochemical impedance spectroscopy indicated that with such sensitivity different types of cancer associated with p53 can be detected at early stages.

The second aim in our study was to prove that the immunosensor was selective and robust. A series of control experiments were performed to guarantee that only samples containing the p53 antigen would yield a positive response in the immunosensor. Indeed, the procedure adopted in the sensing experiments, through which poorly adsorbed analytes could be removed, was proven robust with no false positives for various possible interferences, such as other antigens, glucose, ascorbic acid and uric acid.

### Acknowledgments

This work was supported by FAPESP (2012/17689-9, 2012/15543-7 and 2013/14262-7) and CNPq (Brazil). The authors are thankful to Dr. Nadja K. Wiziack for her help with the antibody and antigen samples.

### References

1. C-C. Wu, C-W. Hsu, C-D. Chen, C-J. Yu, K-P. Chang, D-I. Tai, H-P. Liu, W-H. Su, Y-S. Chang and J-S. Yu, *Mol. Cel. Proteomics*, 2010, **9**, 1100-1117.
2. M. Sana and S. Irshad, *Res.Canc. Tumor*, 2012, **1**, 5-8.
3. P. A. J. Muller and K. H. Vousden, *Cancer Cell*, 2014, **25**, 304-317.
4. P. B. Lippa, L. J. Sokoll and D. W. Chan, *Clin. Chim. Acta*, 2001, **314**, 1-26.
5. S. D. Gan and K. R. Patel, *J. Invest. Dermatol.*, 2013, **133**, 1-3.
6. J. Wang, *Biosensors & Bioelectronics*, 2006, **21**, 1887-1892
7. B. V. Chikkaveeraiah, A. A. Bhirde, N. Y. Morgan, H. S. Eden and X. Chen, *ACS Nano* 2012, **6**, 6546-6561.
8. A. Warsinke; A. Benkert and F. W. Scheller, *J. Anal. Chem.*, 2000, **366**, 622–634.

9. C. K. Tang, A. Vaze and J. F. Rusling, *Anal. Methods*, 2014, **6**, 8878-8881.
10. C. Zong, J. Wu, C. Wang, H. Ju and F. Yan, *Anal. Chem.*, 2012, **84**, 2410-2415.
11. I. Al-Ogaidi, H. Gou, Z. P. Aguilar, S. Guo, A. K. Melconian, A. K. A. Al-Kazaz, F. Meng and N. Wu, *Chem. Commun. (Cambridge, U. K.)*, 2014, **50**, 1344-1346.
12. L. Su, L. Zou, C-C. Wong, W-L. Wong, F. Wei, K-Y. Wong, R. S. S. Wu and M. Yang, *Biosensors & Bioelectronics*, 2013, **46**, 155-161.
13. L. Loo, J. A. Capobianco, W. Wu, X. Gao, W. Y. Shih, W-H. Shih, K. Pourrezaei, M. K. Robinson and G. P. Adams, *Anal. Chem.*, 2011, **83**, 3392-3397.
14. M. Yang, X. Yi, J. Wang and F. Zhou, *Analyst*, 2014, 139, 1814-1825.
15. W-C. Law, K-T. Yong, A. Baev and P. N. Prasad, *ACS Nano*, 2011, **5**, 4858-4864.
16. S. Ishihara, J. Labuta, W. Van Rossom, D. Ishikawa, K. Minami, J. P. Hill and K. Ariga, *Phys. Chem. Chem. Phys.*, 2014, **16**, 9713-9746.
17. J. C. Soares, F. M. Shimizu, A. C. Soares, L. Caseli, J. Ferreira and O. N. Oliveira Jr, *ACS Appl. Mater. Interfaces*, 2015, **7**, 11833-11841.
18. Y. Xie, A. Chen, D. Du and Y. Lin, *Anal. Chim. Acta*, 2011, **699**, 44-48.
19. A. C. Soares, J. C. Soares, F. M. Shimizu, M. E. Melendez, A. L. Carvalho and O. N. Oliveira Jr, *ACS Appl. Mater. Interfaces*, 2015, **7**, 25930-25937.
20. F. Xiao, N. Zhang, H. Gu, M. Qian, J. Bai, W. Zhang and L. Jin, *Talanta*, 2011, **84**, 204-211.
21. T. Wink, S. J. van Zuilen, A. Bult and W. P. Van Bennekom, *Analyst*, 1997, **122**, 43R-50R.
22. H. Chen, X. Guo, *Small*, 2013, **9**, 1144-1159.
23. G. Decher, J. D. Hong and J. Schmitt, *Thin Solid Films*, 1992, **210-211**, 831-835.
24. K. Ariga, Y. Yamauchi, G. Rydzek, Q. Ji, Y. Yonamine, K. C. W. Wu and J. P. Hill, *Chem. Lett.*, 2014, **43**, 36-68.
25. G. Rydzek, Q. Ji, M. Li, P. Schaaf, J. P. Hill, F. Boulmedais and K. Ariga, *Nano Today*, 2015, **10**, 138-167.

26. X. Wang, F. Chen, K. Zhu, Q. Xu and M. Tang, *Anal. Chim. Acta*, 2013, **765**, 63-69.
27. W. Zhou, Y. Ma, H. Yang, Y. Ding and X. Luo, *Int. J. Nanomed.*, 2011, **6**, 381-386.
28. S. Han, S. K. Kim, K. Park, S. Y. Yi, H-J. Park, H-K. Lyu, M. Kim and B. H. Chung, *Anal. Chim. Acta*, 2010, **665**, 79-83.
29. G. H. Yan, D. Xing, S. C. Tan and Q. Chen, *J. Immunol. Methods*, 2004, **288**, 47-54.
30. Y. Zhou, Z. Wang, Q. Zhang, W. Ruan and L. Liu, *IEEE Sens. J.*, 2009, **9**, 246-254.
31. M. Yue, J. C. Stachowiack, H. Lin, R. Datar, R. Cote and A. Majumdar, *Nano Lett.*, 2008, **8**, 520-524.
32. Y. Lee, S. Jeon and W. Moon, *J. Assoc. Lab. Autom.*, 2008, **13**, 259-264.
33. B. M. Cerrutti, M. L. Moraes, S. H. Pulcinelli and C. V. Santilli, *Biosensor & Bioelectronics*, 2015, **71**, 420-426.
34. O. Ouerghi, A. Touhami, A. Othmane, H. Ben Ouada, C. Martelet, C. Fretigny and N. Jaffrezic-Renault, *Biomol. Eng.*, 2002, **19 (2-6)**, 183-188.
35. I. Langmuir, *J. Am. Chem. Soc.*, 1918, **40**, 1361-1403.
36. G. P. Jeppu and T. P. Clement, *J. Contam. Hydrol.*, 2012, **129**, 46-53.
37. A. W. Adamson, A. P. Gast, *Physical Chemistry of Surface*, John Wiley & Sons, Los Angeles, 6th edn, 1997.
38. E. Turiel, C. Perez-Conde and A. Martin-Esteban, *Analyst*, 2003, **128**, 137-141.
39. P. Zhang and L. Wang, *Sep. Purif. Technol.*, 2010, **70 (3)**, 367-371.
40. M. Raposo and O. N. Oliveira Jr, *Langmuir*, 2000, **16**, 2839-2845.
41. F. V. Paulovich, M. L. Moraes, R. M. Maki, M. Ferreira, O. N. Oliveira Jr and M. C. F. de Oliveira, *Analyst*, 2011, **136**, 1344-1350.
42. O. N. Oliveira Jr, T. T. A. T. Neves, F. V. Paulovich and M. C. F. Oliveira, *Chem. Lett.* 2014, **11**, 1672-1679

43. R. Minghim, F. V. Paulovich and A. Lopes, A. IS&T/SPIE Symposium on Electronic Imaging, San Jose -CA, San Jose -CA, 2006, S1-S2.
44. N. B. Colthup, L. H. Daly, *Introduction to Infrared and Raman Spectroscopy*, Academic Press, New York, 3rd edn, 1990.
45. A. Wieckowski, C. Korzeniewski, B. Braunschweig, B. *Vibrational Spectroscopy at Electrified Interfaces*, Wiley, Hoboken, 2013
46. G. Sauerbrey, *Zeit. fur Phys.*, 1959, **155**, 206–22.
47. C. A. Silva, T. M. Nobre, F. J. Pavinatto and O.N. Oliveira Jr., *J. Colloid Interface Sci.*, 2012, **376**, 289–295.
48. W. Szymańska, H. Radecka, J. Radecki and R. Kaliszan, *Biosensors and Bioelectronics* 2007, **22**, 1955-1960.
49. E. Sen, U. Gonullu and N. Akar, *Tuberk Toraks.*, 2005, **53**, 231-7.
50. O. B. Silva, S. A. S. Machado, *Anal. Methods*, 2012, **4**, 2348-2354.